Oxide Modules

Le, Thanh Hung; Van Nong, Ngo; Pryds, Nini

Published in:
Advanced Thermoelectrics: Materials, Contacts, Devices, and Systems

Publication date:
2018

Document Version
Peer reviewed version

Chapter 22

Oxide Modules

Le Thanh Hung, Ngo Van Nong, and Nini Pryds

Contents

22.1 Introduction

TE oxides have been considered as promising materials due to their nontoxicity, low cost, and chemical stability at high temperatures [1–3]. Studied results show great potential for applications in TEG at high temperature and have thus drawn much attention over the years. This chapter targets to summarize the research and development of exploring the usage of TE oxide-based materials for high-temperature TEGs. The performance of oxide-based materials and devices in the first part of this chapter will be considered under the ideal theoretical condition of no parasitic losses and disregard other factors such as mechanical properties, thermal expansion coefficient, and chemical stability.

Changed to "oxide-based materials and devices" OK?

In general, the conversion efficiency of a TEG is governed by device figure of merit ZT.

$$ZT = \frac{S^2 T}{KR}, \tag{22.1}$$

where S, K and R are the total Seebeck coefficient, the total thermal conductance, and the total resistance of the module, respectively.

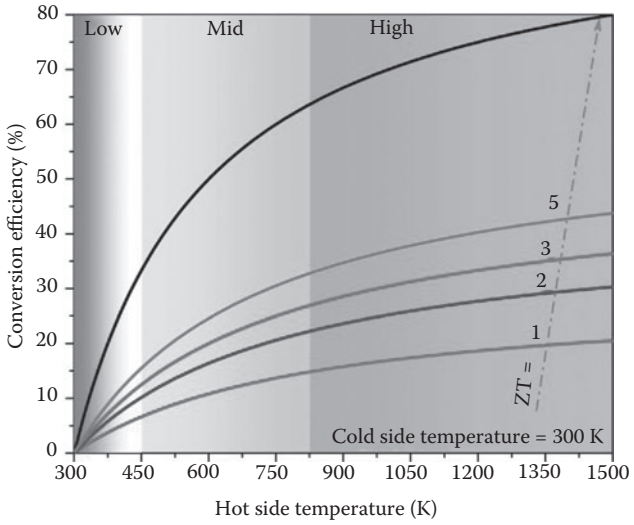

FIGURE 22.1 Calculated conversion heat–electricity efficiency as a function of temperature and device figure of merit.

The maximum conversion efficiency of TE module is often given as

$$\eta_{max} = \frac{T_h - T_c}{T_h} \frac{\sqrt{1+Z\bar{T}} - 1}{\sqrt{1+Z\bar{T}} + (T_c/T_h)}. \quad (22.2)$$

Please check if the correction ma[illegible] this eq[illegible]tion is okay or [illegible]nt to retain the original format.

The first term of Equation 22.2 is known as the Carnot efficiency, which is the upper limit conversion efficiency at infinite *ZT*, as shown in Figure 22.1. The second term is the contribution by the intrinsic properties of the TE materials, i.e., Seebeck coefficient and electrical and thermal conductivities. It is clearly seen that the maximum conversion efficiency of module increases by increasing the hot side temperature as a result of the contribution from the first term in Equation 22.2, i.e., Carnot efficiency. For high-temperature TEG application in air, devices fabricated from intermetallic compounds often show oxidation, sublimation, and volatility processes in the high-temperature range [4,5]. Therefore, encapsulation is needed to protect the devices. By considering the reasons mentioned earlier, the high-temperature oxide TE module is of great interest in high-temperature heat–electricity conversion, e.g., waste heat recovery from steel industrial and thermal power plants.

22.2 Calculated Efficiency of All Oxide Materials and Modules

There have been many studies over the years on the development of high-performance TE oxide materials. Figure 22.2a and b shows a selection of the state-of-the-art material figure of merit *ZT* ($Z = S^2/\rho\kappa$), for p-type and n-type oxide materials. Oxide materials exhibit widely their peak *ZT* values ranging from 0.1 at 1173 K for NiO [6], $NdCoO_3$ [7], and $LaSrCuO_4$ [8], 0.2 for $Ca_3Co_2O_6$ [9], and 0.65 for $Ca_3Co_4O_9$ nanocomposite [10] at 1173 K and to the value of

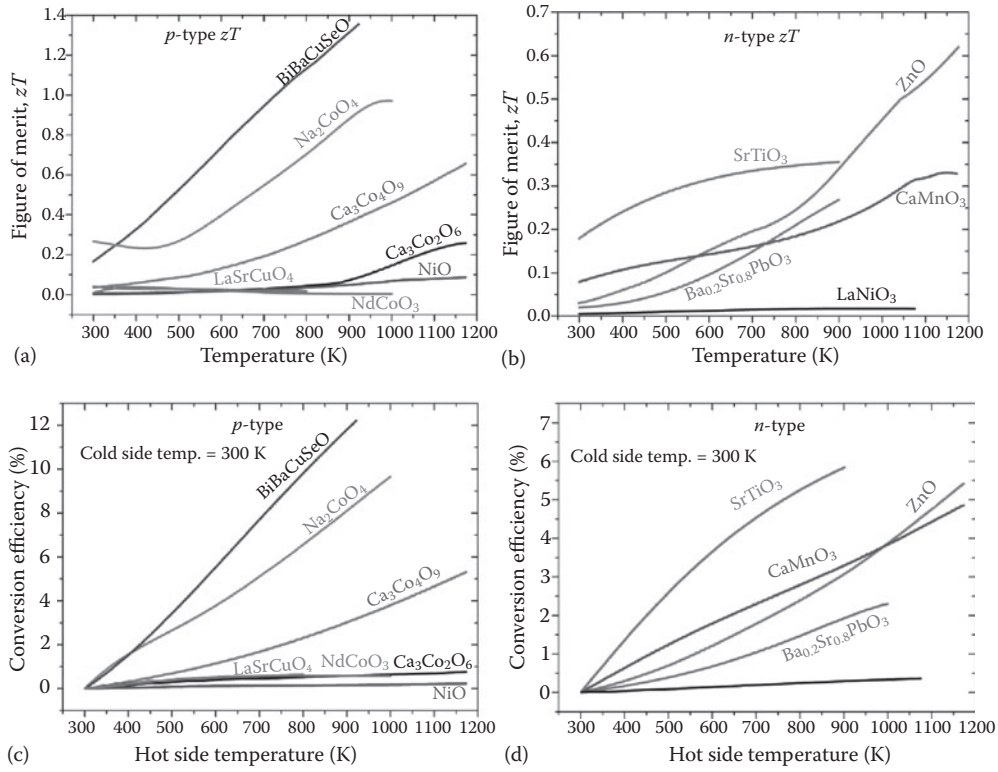

FIGURE 22.2 Material figure of merit *ZT* of state-of-the-art oxide material (a) p-type and (b) n-type. The calculated maximum efficiency of single (c) p-type and (d) n-type TE oxide elements as a function of hot-side temperature.

close to 1 at 1000 K for Na_2CoO_4 [11] and over 1 at 900 K for BiCuSeO [12]. For n-type oxide materials, the $LaNiO_3$ [13,14] attains the lowest magnitude of $ZT < 0.05$ in the temperature range of 300–1100 K. Perovskites $BaSrPbO_3$ [15], $CaMnO_3$ [16], and $SrTiO_3$ [17] obtain a medium *ZT* value of around 0.3 at 1173 K, while dual doped ZnO [18] presents the highest peak *ZT* value of 0.65 at 1173 K. Since most oxide materials (except BiCuSeO) have a small *ZT* value in the low and mid-temperature ranges of 300–700 K, TEG-based oxide has gained much interest mainly for high-temperature waste heat harvesting applications, e.g., steel or cement industrials.

To estimate the efficiency of oxide materials under the actual working condition, we have used numerical modeling [1,19–21].

The efficiency of a single material can be expressed as [1,20,21]

$$\eta = 1 - \frac{S_c T_c + 1/u_c}{S_h T_h + 1/u_h}, \tag{22.3}$$

where S_c, T_c, u_c, S_h, T_h, and u_h are the Seebeck coefficient, temperature, and reduced current density at the cold- (subscript by c) and hot-side (subscript by h) temperatures, respectively. The relative current density (reduced current

density) $u = J/\kappa\nabla T$ is defined as the ratio of the electrical current density (J) to the conduction heat flux (κ) [1,20,21]. In this calculation, the cold-side temperature is fixed at 300 K while the temperature of the hot side is varied. It should be noted that neither heat losses nor electrical losses are included in these calculations. Therefore, the obtained values can be considered as the upper limit performance achievable from the intrinsic TE properties. Figure 22.2c and d shows the calculated efficiency as a function of the hot-side temperature (cold side fixed at 300 K) for p-type and n-type oxide materials as a single element. For the conversion efficiency of all p-type curves in Figure 22.2c, the order of efficiency values of a single material has a similar tendency with ZT curves, as shown in Figure 22.2a. With the smallest ZT values, NiO, $NdCoO_3$, and $LaSrCuO_4$ have a maximum efficiency of less than 1% in the whole temperature of 300 and 1173 K. Although the ZT value of $Ca_3Co_2O_6$ rapidly increases with increasing temperature (Figure 22.2a), its conversion efficiency is still lower than 1% due to low-performance contribution in the whole temperature range. With the maximum conversion efficiency of 5.4%, the $Ca_3Co_4O_9$ is the most the promising p-type oxide material for temperature region of above 1000 K, while below 1000 K, Na_2CoO_4 and BiCuSeO oxyselenides exhibit conversion efficiencies of 10% and 12%, respectively. As for the n-type, $LaNiO_3$ shows an efficiency value which is lower than 0.1%, while $BaSrPbO_3$ shows a maximum value of around 2%. Interestingly, although the peak ZT of $SrTiO_3$ exhibits lower value, its maximum conversion efficiency is higher than that of dual doped ZnO; it is due to the conversion efficiency results from the accumulated performance of the whole working temperature range. The ZT value of $CaMnO_3$ is higher than that of the dual doped ZnO at temperatures below 600 K, while it is significantly lower in the temperature region of above 600 K, as shown in Figure 22.2b. However, the efficiency value of $CaMnO_3$ is higher than the efficiency of dual doped ZnO in the whole temperature range from 300 to 1000 K. In fact, the total conversion efficiency can be calculated as $\eta = \eta_c\eta_r$, where $\eta_c = (T_h - T_c)/T_c$ is the Carnot efficiency, and $\eta_r = [1 - u\,(S/z)] / [1 + (1/uST)]$ is the reduced efficiency [21]. Mathematically, η_r maximizes when $u = \left(\sqrt{1+zT} - 1\right)/ST = s$, which is called the compatibility factor [21,22]. In case where $s = u$, the material can obtain the maximum achievable total conversion efficiency. The smaller the value of $(s - u)$, the larger achievable total conversion efficiency is obtained. Therefore, s and u values are important parameters and are needed to be considered for designing high-efficiency materials [1,23,24].

Please check if the correction made on this equation is okay or you want to retain the original format.

By connecting the p-type and n-type oxide elements, the efficiency of a unicouple can be computed as

$$\eta_{\text{unicouple}} = 1 - \frac{S_{c,p}T_{c,p} + 1/u_{c,p} - S_{c,n}T_{c,n} - 1/u_{c,n}}{S_{h,p}T_{h,p} + 1/u_{h,p} - S_{h,n}T_{h,n} - 1/u_{h,n}}, \qquad (22.4)$$

Please check if the correction made on this equation is okay or you want to retain the original format.

where the subscripts n and p symbolize the n- and p-type legs. The calculated efficiency using Equation 22.4 for some promising unicouple-based oxide TE materials are summarized in Table 22.1. The hot-side temperature is defined by

TABLE 22.1 Calculated Maximum Conversion Efficiency of Unicouples with Various Maximum Hot-Side Temperatures and the Combination of p–n Oxide Leg

T_{hot} = 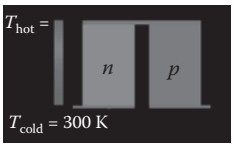	$Ca_3Co_4O_9$ (T_{hot}/1173 K) (%)	$Ca_3Co_2O_6$ (T_{hot}/1173 K) (%)	Na_2CoO_4 (T_{hot}/1000 K) (%)	BiCuSeO (T_{hot}/900 K) (%)
ZnO (T_{hot}/1173 K)	5.3	1.4	6.1	5.2
$CaMnO_3$ (T_{hot}/1173 K)	5.0	1.7	5.7	5.1
$Ba_{0.2}Sr_{0.8}PbO_3$ (T_{hot}/1000 K)	2.9	0.9	3.1	3.6
$SrTiO_3$ (T_{hot}/900 K)	4.1	0.89	7.0	7.9

the limited stability of the comprising TE materials, e.g., 900 K for any unicouple made by p-BiCuSeO and n-$SrTiO_3$. It can be seen that the combination of p- and n-type oxides resulted in different conversion efficiencies; the unicouples with $Ca_3Co_2O_6$ show the smallest values ranging from 0.9% to 1.7%; in contrast, the unicouple of p-BiCuSeO and n-$SrTiO_3$ exhibits the highest conversion efficiency of up to 7.9%. For the highest hot-side temperature of 1173 K, the p-type $Ca_3Co_4O_9$ combines with either n-type ZnO or $CaMnO_3$, showing a 5% efficiency, which is comparable with that of a current commercially available TE module based on Bi-Te materials. These results suggest that oxide TE materials have a great potential for high-temperature TEG for waste heat harvesting.

Changed to "combines with either n-type ZnO... a current co... cially av... ble" OK?

22.3 Oxide Module Construction and Characterization

Figure 22.3 shows the process steps for a typical module fabrication and characterization. The p- and n-type material processing first optimizes their

Changed to "The p- and n-type mat... ocessing f... st o...imizes thei... oper-ties." OK?

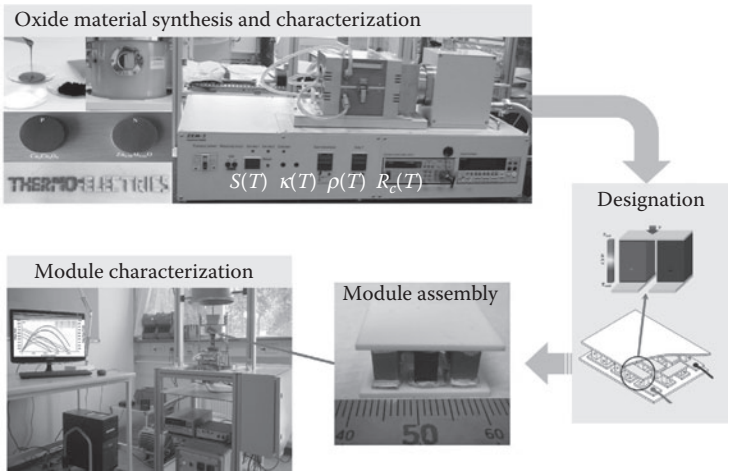

FIGURE 22.3 Schematic of the whole TE oxide module construction process: from material synthesis and characterization, modeling design, to build up and test module.

TE properties. The solid-state reaction is the preferred synthesis method for fabricating the oxide TE powder materials. For densification, hot press or SPS techniques are often used [19,25–28]. Following the synthesis and the densification, the TE properties of the materials are measured as a function of the temperature and fed into a numerical model, where the optimal output performance of the module is then calculated for a given optimized geometry of the legs and number of p–n couples [25]. The p- and n-type legs were then cut into the dimensions suggested by the modeling results. The unicouple contains two TE materials, n- and p-type, coupled together with a metal electrode. Silver (Ag) is the most used material for electrodes in module assembly [8,25–45] since it has high electrical and thermal conductivities and can resist high temperature in air.

The joining of Ag electrodes with TE legs is often done by the brazing method with filler materials which can be either pure Ag [25,28,35], Pt paste [29], Ag paste [31,33,38–45] or a mixture of Ag and oxide powder [30,32,37] depending on the materials in use. Joining by diffusion between oxide materials and Ag electrodes was also suggested, as described by Souma et al. [26,27]. This technique can tightly join two materials, be faster than brazing joining method, and does not require a filler metal. One of the crucial demands from the joining contacts is low electrical resistance and stability. A low resistance and stable contact are required since they ensure high performance and long-term stability of the TE module. Figure 22.4 shows typical experimental results of contact resistances of single p-type $Ca_3Co_4O_9$, single-segmented p-type $Ca_3Co_4O_9$/HH alloy, and n-type-doped ZnO oxide with Ag electrode using brazing joining method [19,25]. There is no sign of cracks or air gap observed at the interfaces, which results in low contact resistance

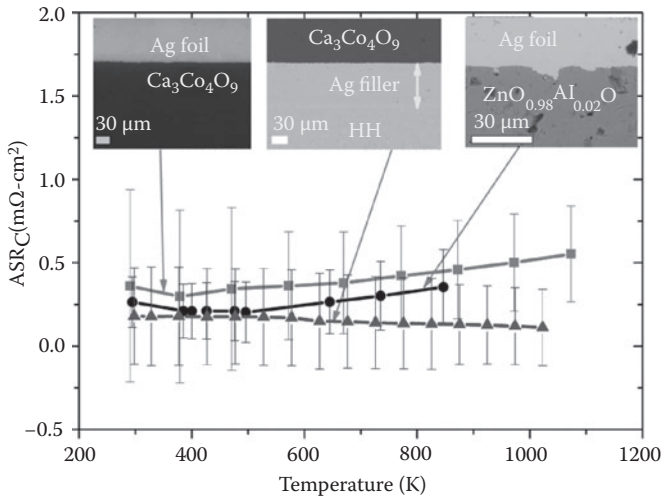

FIGURE 22.4 Picture of interface and contact resistance of the Ag with p-type and n-type oxide materials. (Hung, L. T. et al.: Segmented thermoelectric oxide-based module for high-temperature waste heat harvesting. *Energy Technology*. 2015. 3. 1143–1151. Copyright Wiley-VCH Verlag GmbH & Co. KGaA. Reproduced with permission.)

in the range of 100–500 μΩ cm^2 [19,25]. The entire module with the electrical insulation substrate is finally assembled by hot press method. It is crucial that each step in Figure 22.3 should be properly done, and any failure in one of the steps must be carefully checked or come back to optimize the previous steps.

22.4 All Oxide Thermoelectric Modules

Table 22.2 is a summary of TE oxide modules reported in the literature over the last 16 years. The size of those modules is varied largely from a TEG module comprising of a single unicouple up to 140 unicouples. Although the ZT value of 0.93 at 960 K of the p-type $NaCo_2O_4$ is very high, only a few oxide modules have been studied using $NaCo_2O_4$ [26,27,36] as p-type leg. The p-type $Ca_3Co_4O_9$ is mostly used because this material is highly stable at a high temperature in air [46]. For n-type, $CaMnO_3$ or doped ZnO are dominated materials since the higher ZT n-type $SrTiO_3$ is not stable in air at an elevated temperature [2]. As shown in Table 22.2, the power generation characteristics have been conducted under various conditions of the hot- and cold-side temperatures, resulting in differences in open circuit voltage and maximum output power. To give a comparison of studied oxide modules, the power density is often used [25,39,45]. However, one should be careful when using the value of power density, which might also lead to an unreasonable conclusion, because the power density depends on the length and the number of the TE legs. A more clear explanation can be described in the following.

Changed to "resulting in differences in open circuit voltage and maximum output power" OK?

The performance of module comprising p–n couples can be expressed in terms of the output voltage and current values. The open circuit voltage V_{OC} can be directly calculated from the definition of the Seebeck coefficient as [47]

$$V_{OC} = n\int_{T_c}^{T_h} \{S_p(T) - S_n(T)\}\,dT, \tag{22.5}$$

where n is the number of p–n couples, S_p and S_n are the Seebeck coefficients of p- and n-type legs, respectively. Moreover, the value of the electric current I can be calculated from Ohm's law as

$$I = \frac{V_{OC}}{R_{int} + R_{Load}}, \tag{22.6}$$

where R_{int} is the total of the internal resistances of the module that is contributed by the sum of the resistances of the p–n legs, and R_{Load} is the external resistive load. The internal resistance can be described as $R_{int} = R_{legs} + R_C$,

The font size has been reduced to fit Table 22.2 as formatted. Is this OK?

TABLE 22.2 Power Generation Characteristics of Oxide-Based TE Modules Reported in the Literature

Ref.	Year	Materials	No. of p–n Couples	Jointing Technique	T_{hot} (K)	ΔT (K)	V_{OC} (V)	V_{OC}/ Couples (V)	P_{max} (mW)	Leg Size (mm)	Power Density (mW/cm²)	Efficiency (%)	
												Cal	Mea
[28]	2001	p-$Li_{0.025}Ni_{0.975}O$ n-$Ba_{0.2}Sr_{0.8}PbO_3$	1	Cosintering, cold side Ag paste	978	552	0.12	0.12	7.91	3 × 4 × 14	32.9	0.64	–
[28]	2001	p-$Li_{0.025}Ni_{0.975}O$ n-$Ba_{0.2}Sr_{0.8}PbO_3$	4	Cosintering, cold side Ag paste	1164	539	0.4	0.1	34.4	3 × 4 × 14	35.8	–	–
Matsubara et al. [29]	2001	p-$Ca_{2.75}Gd_{0.25}Co_4O_9$ n-$Ca_{0.92}La_{0.08}MnO_3$	8	Pt paste	1046	390	0.98	0.12	63.5	3 × 3 × 25	44.1	1.1	–
Funahashi et al. [30]	2004	p-$Ca_{2.7}Bi_{0.3}Co_4O_9$ n-$La_{0.9}Bi_{0.1}NiO_3$	1	Ag paste, 6 wt.% oxide powder	1073	500	0.1	0.1	94	3.7 × 4–4.53 × 4.7	317–280[a]	–	–
Reddy et al. [31]	2005	p-$Ca_3Co_4O_9$ n-$Ca_{0.95}Smo_{0.05}MnO_3$	2	Ag paste	1025	925	0.4	0.2	31.5–24.5	4 × 4 × 5	98.4	–	–
Funahashi et al. [32]	2006	p-$Ca_{2.7}Bi_{0.3}Co_4O_9$ n-$La_{0.9}Bi_{0.1}NiO_3$	140	Ag paste, 6 wt.% oxide	1072	551	4.5	0.03	150	1.3 × 1.3 × 5	31.7	1.3	–
Souma et al. [26]	2006	p-$NaCo_2O_4$ n-$Zn_{0.98}Al_{0.02}O$	12	Diffusion welding	839	462	0.8	0.06	58	3 × 4 × 10	20.1	–	–
Urata et al. [33]	2006	p-$Ca_{2.7}Bi_{0.3}Co_4O_9$ n-$CaMn_{0.98}Mo_{0.02}O_3$	8	Ag paste	897	565	1	0.12	170	5 × 5 × 4.5	42.5	–	–
Funahashi et al. [34]	2007	p-$Ca_{2.7}Bi_{0.3}Co_4O_9$ n-$La_{0.9}Bi_{0.1}NiO_3$	1	Ag paste	1073	500	0.1	0.1	177	3.7 × 4–4.53 × 4.7	528-598[a]	–	–
Urata et al. [35]	2007	p-$Ca_{2.7}Bi_{0.3}Co_4O_9$ n-$CaMn_{0.98}Mo_{0.02}O_3$	8	Ag	1273	975	0.7	0.09	340	5 × 5 × 4.5	85	–	–
Souma et al. [27]	2008	p-$NaCo_2O_4$ n-$Zn_{0.98}Al_{0.02}O$	12	Diffusion welding	934	455	0.8	0.067	52.5	3 × 4 × 10	18.2	–	–
Park et al. [36]	2009	p-$Na(Co_{0.95}Ni_{0.05})_2O_4$ n-$Zn_{0.99}Sn_{0.01}O$	1	Ag paste	923	422	0.14	0.14	0.027	7 × 7 × 17	0.03	–	–
Tomeš et al. [8]	2010	p-$La_{1.98}Sr_{0.02}CuO_4$ n-$CaMn_{0.98}Mo_{0.02}O_3$	2	Ag paste	941	622	0.464	0.23	88.8	4.5 × 4.5 × 5	109.6	–	0.073

(*Continued*)

TABLE 22.2 (CONTINUED) Power Generation Characteristics of Oxide-Based TE Modules Reported in the Literature

Ref.	Year	Materials	No. of p–n Couples	Jointing Technique	T_{hot} (K)	ΔT (K)	V_{OC} (V)	V_{OC}/ Couples (V)	P_{max} (mW)	Leg Size (mm)	Power Density (mW/cm^2)	Efficiency (%)	
												Cal	Mea
Tomeš et al. [37]	2010	p-$GdCo_{0.95}Ni_{0.05}O_3$ n-$CaMn_{0.98}Mo_{0.02}O_3$	2	Ag/CuO paste	800	500	0.34	0.17	40	4 × 4 × 5	62.5	–	–
Choi et al. [38]	2011	p-$Ca_3Co_4O_9$ n-$(ZnO)_7In_2O_3$	44	Ag paste	1100	673	1.8	0.04	423	15 × 15 × 27	2.1	–	–
Lim et al. [39]	2011	p-$Ca_3Co_4O_9$ n-$Ca_{0.9}Nd_{0.1}MnO_3$	1	Ag paste	1175	727	0.19	0.19	95	8.5 × 6 × 10	93.2	–	–
Inagoya et al. [40]	2011	p-$Nd_{0.995}Ca_{0.005}CoO_3$ n-$LaCo_{0.99}Mn_{0.01}O_3$	10	Ag paste	704	399	1	0.1	44	23 mm^2 × 20	9.6	–	–
Han et al. [41]	2011	p-$Ca_3Co_{3.8}Ag_{0.2}O_9$ n-$Ca_{0.98}Sm_{0.02}O_3$	2	Ag paste	873	523	0.33	0.16	36.8	3 × 6 × 6	51.1	–	–
Funahashi [42]	2011	p-$Ca_{2.7}Bi_{0.3}Co_4O_9$ n-$Ca_{0.9}Yb_{0.1}MnO_3$	108	Ag paste	873	400	10.5	0.097	12000	7 × 3.5 × 5	226.7[b]	–	–
Park and Lee [43]	2013	p-$Ca_{2.76}Cu_{0.24}Co_4O_9$ n-$Ca_{0.8}Dy_{0.2}MnO_3$	4	Ag paste	937	321	0.28	0.07	31	7 × 9 × 25	6.15	–	–
Mele et al. [44]	2014	p-$Ca_3Co_4O_9$ n-$Zn_{0.98}Al_{0.02}O$	6	Ag paste	773	248	0.12	0.02	2.26	4 × 4 × 10	1.2	–	–
Saucke et al. [45]	2015	p-$Ca_3Co_{3.9}O_{9.3}$ n-$CaMn_{0.97}W_{0.03}O_3$	2	Ag paste	1051	727	0.36	0.18	200.4	40.77 mm^2 × 4	491[c]	1.08	1.08
Hung et al. [25]	2015	p-$Ca_3Co_4O_9$ n-$Zn_{0.98}Al_{0.02}O$	4	Ag	1173	700	0.67	0.17	256	4 × 4 × 8	200	0.72	0.37
Hung et al. [25]	2015	p-HH/$Ca_3Co_4O_9$ n-$Zn_{0.98}Al_{0.02}O$	4	Ag	1173	700	0.76	0.19	829	4 × 4 × 8	650	1.8	1.16

[a] The reported data from the same author is somewhat inconsistent. In addition, the theoretical calculation under ideal conditions, i.e., no losses shows the maximum power density of 200 mW/cm$_2$. Therefore, experimental needs to be confirmed.
[b] The value is calculated based on the experimental data in the article.
[c] The length of the legs is computed from the ratio of volume and area.

and R_{Load}, where R_{legs} is the sum of the resistances of the p–n legs without metal electrodes, and R_C is the contact resistance contribution from all interfacial contact between electrodes and the legs. The output power as a function of electric current and the resistive load is given by

$$P = I^2 R_{Load} = V_{OC}^2 \left[\frac{R_{Load}}{(R_{int} + R_{Load})^2} \right]. \tag{22.7}$$

The maximum output power is obtained when the external load resistance is equal to the internal resistance ($R_{int} = R_{Load}$):

$$P_{Max} = \frac{V_{OC}^2}{4R_{int}} = \frac{V_{OC}^2}{4R_C + 4R_{legs}} = \frac{V_{OC}^2}{4R_C + 4n\left[\rho_p \left(l_p / A_p\right) + \rho_n \left(l_n / A_n\right)\right]}, \tag{22.8}$$

Please check if the correction made on this equation is okay or you want to revert to the original format.

where ρ_p, ρ_n, A_p, A_n, l_p, and l_n are values of the electrical resistivity, cross-sectional area, and length of the p-type (subscript p) and n-type (subscript by n), respectively.

It is clearly seen from Equations 22.5 and 22.8 that the maximum output power is proportional to the total number of the p–n couples and Seebeck coefficient, but its magnitude is inversely proportional to the length of p-type and n-type legs, i.e., the shorter length will provide higher output power.

Changed to "divided by the total area times the number of legs"

The power density is defined as the ratio of P_{max} divided by the total area times the number of legs $n(A_p + A_n)$:

$$P_{density} = \frac{P_{Max}}{n(A_p + A_n)}. \tag{22.9}$$

Equations 22.8 and 22.9 indicate that the power density increases by decreasing the length of the TE legs as result of increasing P_{max}. As presented in Table 22.2, the highest value of power density falls on the modules with a short leg length such as those in the studies by Funahashi [42] and Saucke et al. In contrast, the module constructed from a longer length has a low value of powder density, e.g., from the studies by Souma et al. [26] and Matsubara et al. [29].

To compare the performance of modules, the conversion efficiency η, which is the ratio of electric power to the total heat input, is a more appropriate way to use [47]. η can be defined as:

$$\eta = \frac{P}{Q_h} = \frac{P}{K(T_h - T_c) + V_{OC} T_h I - 0.5 I^2 R_{legs}}. \tag{22.10}$$

Equations 22.7 and 22.10 imply that the efficiency value of the devices is independent from the length of TE legs. As can be seen from Table 22.2, there

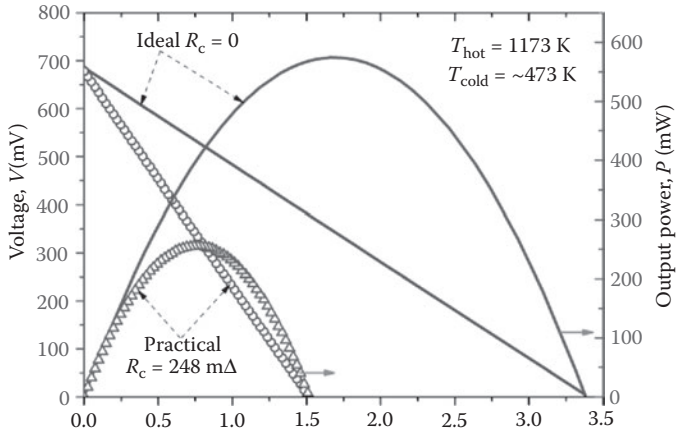

FIGURE 22.5 Experimental (*open circle and triangle*) and ideal conditions (*solid line*) of voltages and output power for the 4 p–n couples comprising from n-type $Zn_{0.98}Al_{0.02}$ and p-type $Ca_3Co_4O_9$. (Hung, L. T. et al.: Segmented thermoelectric oxide-based module for high-temperature waste heat harvesting. *Energy Technology*. 2015. 3. 1143–1151. Copyright Wiley-VCH Verlag GmbH & Co. KGaA. Reproduced with permission.)

is only a few research reported on the value of efficiency making it difficult to collect the data. This may be because the measurement of the heat flux on the hot side of the TEG is complicated especially in the high-temperature range. The maximum obtained efficiency value of all studied data is currently less than 2%, and this value is far from theoretical calculation values, as listed in Table 22.1. One of the main sources, which lead to low conversion efficiency value, is the contact resistances, i.e., high electrical and thermal contact resistances at the interface of oxide materials and metal electrodes. In the experiment, the contact resistance of oxide–metal is in the range of 25–400 μΩ cm^2 for Ag and $Ca_3Co_4O_9$ [19,25,45], and it is in the range of 100–500 μΩ cm^2 for Ag and doped ZnO [25]. Figure 22.5 gives an example of how contact resistance influences the output performance of the oxide module. An interfacial contact resistance of 248 mΩ leads to the suppression of the maximum output power from 575 mW for the ideal theoretical condition to 256 mW for the practically measured condition. Therefore, the study of interfacial contact resistance is a critical area of research to improve the performance of any TEG. In summary, although considerable attempts have been made to produce highly efficient TE oxide modules, the performance of those reported oxide TEGs is still low due to the low performance of oxide materials in the low-mid temperature and high interfacial oxide–metal contact resistances.

22.5 Segmented Oxide-Based Modules

As aforementioned, one of the main drawbacks of reported oxide TEG is the low performance of oxide materials in the temperature range of 300–700 K. In this context, there are two possible solutions where oxide TEG can be

combined with other materials: either in cascaded or segmented generators. In a cascade generator, the oxide TEG is stacked with other high-performance TEG working at a mid-low temperature that is normally made of alloys. By this way, the performance of the module can be improved with about twice compared to that of single oxide-based module [42]. However, this type of module often requires an additional electronic device to collect the maximum output of two electric circuits in each single stage. The electrical wires are needed for the connection, and hence, a large amount of heat losses exists in electrical connection wires either heat conductance loss due to the low electrical resistivity or Joule heating loss due to the high electrical resistance [48]. In contrast, a segmented TEG requires only a single electric circuit. In a segmented TE module, the p-type and/or n-type legs are designed by a segmentation of different materials with their highest value of *ZT*. One of the criteria to ensure an improvement in efficiency is that the difference in compatibility factor $\left(s = \left(\sqrt{1+zT}-1\right)/T\right)$ values of the selected materials have to be within a factor of two [1,20,22,49]. According to Hung et al. [50], the high conversion efficiency of 12.2% can be achieved in a unicouple of segmented p-type $Ca_3Co_4O_9$ and n-type dual doped ZnO with state-of-the art TE materials of, e.g., BiTe, PbTe, and HH alloys. Figure 22.6 shows the result of a segmented oxide module using n-type $Zn_{0.98}Al_{0.02}O$ and segmented p-type half-Heusler-$Ca_3Co_4O_9$. Its performance was analyzed and compared to nonsegmented module with similar dimension under the same testing conditions. The obtained output power of those modules under the same measurement conditions clearly indicates that segmentation is an effective way to boot up the performance of oxide module. An efficiency of 1.16% is achieved for segmented module, which is three times higher than that of nonsegmented one, as shown in Table 22.2. Furthermore, the conversion

Please check "electrical connection wires either heat conductance loss due to the low electrical resistivity or Joule heating loss due to the high electrical resistance" for corrections or missing text.

Please check if the correction made on equation is okay or you want to retain the original format

Changed to "An efficiency 1.16% is achieved for segmented module" OK?

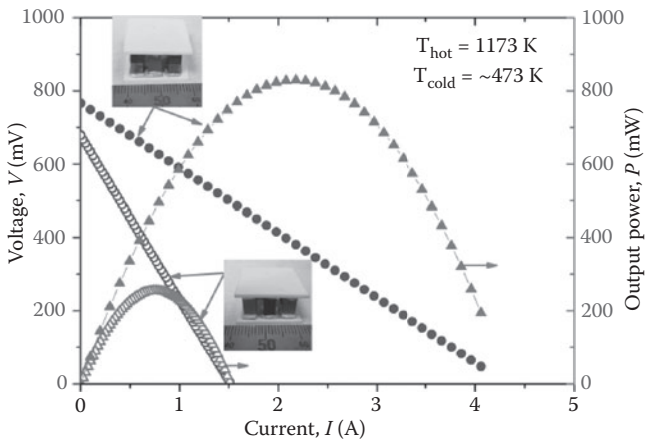

FIGURE 22.6 Power generation characteristics of 4 p–n couples oxide module using n-type $Zn_{0.98}Al_{0.02}$ and p-type $Ca_3Co_4O_9$ and 4 p–n couples segmented oxide module using n-type $Zn_{0.98}Al_{0.02}$ and segmented p-type half-Heusler-$Ca_3Co_4O_9$. (Hung, L. T. et al.: Segmented thermoelectric oxide-based module for high-temperature waste heat harvesting. *Energy Technology*. 2015. 3. 1143–1151. Copyright Wiley-VCH Verlag GmbH & Co. KGaA. Reproduced with permission.)

efficiency of 5% has also been achieved in single p-type segmented leg of misfit-layered cobaltite and HH alloy [19]. In both cases, the segmented legs are highly stable at a high temperature in air.

22.6 Outlook and Challenges

Oxide TE modules have been rapidly developed in the last 16 years with many attempts to improve the conversion efficiency of TEG modules for high-temperature waste heat harvesting. Some of the efforts have been successfully realized, and promising devices are now commercially available [51]. The theoretical calculation has pointed out that TEG with the efficiency of 7.9% could be possibly obtained in oxide materials if parasitic losses can be minimized.

There is a big gap existing between the performance of materials and performance of devices. Although many studies have been conducted to improve the performance of oxide materials, the maximum conversion efficiency of current oxide module is still lower than 2%. In fact, TE properties of oxide materials are studied as a function of temperature, thermal cycling, or heat treatment duration in which all parasitic losses were disregarded. In practice, oxide TE legs in module operate under a large temperature gradient and generating power conditions with the contribution of electrical and thermal losses. Thus, studying the performance of oxide material under working conditions would help reduce the currently existing gap of materials and devices.

We have also clearly pointed out that one of the main sources leading to the decrease in the performance of oxide TEG is the contact resistances. Understanding the contact resistance requires more study to theoretically clarify the origin of the resistance and to not only make a good electrical connection but also have durability from thermal cycling and large temperature span. Also, studying metal–oxide interfacial contact resistances under module level could be an important topic.

Changed to "to theoretically clarify the origin of the resistance [illegible] to not only [illegible] a good electrical connection but also have durability from thermal cycling and large temperature span." OK?

The combination of taking the advantages of oxides and other intermetallic alloys in segmented TEG has been realized as one of the most efficient ways to produce high efficiency. The stable and high conversion efficiency of 5% was achieved on segmented p-type-based oxide materials. The future study, therefore, should target segmented n-type oxide materials.

Please check if "The combination of taking the advantages of oxides and other intermetallic alloys in segmented TEG ha[illegible] realized" ca[illegible] be [illegible]hanged to "T[illegible]dvantage of the combination of oxides and other intermetallic alloys in segmented TEG has been realized".

References

1. Hung, L. T., Van Nong, N., Linderoth, S., and Pryds, N. Segmentation of low-cost high efficiency oxide-based thermoelectric materials. *Phys Status Solidi* 2015;212:767–74.
2. Koumoto, K., Wang, Y., Zhang, R., Kosuga, A., and Funahashi, R. Oxide thermoelectric materials: A nanostructuring approach. *Annu Rev Mater Res* 2010;40:363–94.
3. Koumoto, K. *Thermoelectrics Handbook: Macro to Nano*, 2006.
4. Yang, J., and Caillat, T. Thermoelectric materials for space and automotive power generation. *MRS Bull* 2006;31:224–9.

Please provide publisher name and location.

5. Kambe, M., Jinushi, T., and Ishijima, Z. Encapsulated thermoelectric modules and compliant pads for advanced thermoelectric systems. *J Electron Mater* 2010;39:1418–21.
6. Shin, W., and Murayama, N. Li-doped nickel oxide as a thermoelectric material. *Japanese J Appl Phys, Part 2 Lett* 1999;38:1336–8.
7. Moon, J.-W., Seo, W.-S., Okabe, H., Okawa, T., and Koumoto, K. Ca-doped $RCoO_3$ (R = Gd, Sm, Nd, Pr) as thermoelectric materials. *J Mater Chem* 2000;10:2007–9.
8. Tomeš, P., Trottmann, M., Suter, C., Aguirre, M. H., Steinfeld, A., Haueter, P. et al. Thermoelectric Oxide Modules (TOMs) for the direct conversion of simulated solar radiation into electrical energy. *Materials (Basel)* 2010;3:2801–14.
9. Nong, N. V., and Ohtaki, M. Thermoelectric properties and local electronic structure of rare earth-doped $Ca_3Co_2O_6$. *2006 25th International Conference on Thermoelectrics* 2006:62–5.
10. Van Nong, N., Pryds, N., Linderoth, S., and Ohtaki, M. Enhancement of the thermoelectric performance of p-type layered oxide $Ca_3Co_4O_{(9+\delta)}$ through heavy doping and metallic nanoinclusions. *Adv Mater* 2011;23:2484–90.
11. Ito, M., and Furumoto, D. Microstructure and thermoelectric properties of $Na_xCo_2O_4$/Ag composite synthesized by the polymerized complex method. *J Alloys Compd* 2008;450:517–20.
12. Sui, J., Li, J., He, J., Pei, Y.-L., Berardan, D., Wu, H. et al. Texturation boosts the thermoelectric performance of BiCuSeO oxyselenides. *Energy Environ Sci* 2013;6:2916.
13. Thermoelectric properties of Ni-based oxides 2004;793:1–11.
14. Hsiao, C.-L., Chang, W.-C., and Qi, X. Sol–Gel synthesis and characterisation of nanostructured $LaNiO_{3-x}$ for thermoelectric applications. *Sci Adv Mater* 2014;6:1406–11.
15. Yasukawa, M., and Murayama, N. A promising oxide material for high-temperature thermoelectric energy conversion: $Ba_{1-x}Sr_xPbO_3$ solid solution system. *Mater Sci Eng B* 1998;54:64–9.
16. Bocher, L., Aguirre, M. H., Logvinovich, D., Shkabko, A., Robert, R., Trottmann, M. et al. $CaMn_{1-x}$ Nb_xO_3 ($x \leq 0.08$) perovskite-type phases as promising new high-temperature n-type thermoelectric materials. *Inorg Chem* 2008;47:8077–85.
17. Wang, N., He, H., Ba, Y., Wan, C., and Koumoto, K. Thermoelectric properties of Nb-doped $SrTiO_3$ ceramics enhanced by potassium titanate nanowires addition. *J Ceram Soc Japan* 2010;118:1098–101.
18. Ohtaki, M., Araki, K., and Yamamoto, K. High thermoelectric performance of dually doped ZnO ceramics. *J Electron Mater* 2009;38:1234–8.
19. Hung, L. T., Van Nong, N., Snyder, G. J., Viet, M. H., Balke, B., Han, L. et al. High performance p-type segmented leg of misfit-layered cobaltite and half-Heusler alloy. *Energy Convers Manag* 2015;99:20–7.
20. Ngan, P. H., Christensen, D. V., Snyder, G. J., Hung, L. T., Linderoth, S., Nong, N. V. et al. Towards high efficiency segmented thermoelectric unicouples. *Phys Status Solidi* 2014;211:9–17.
21. Snyder, G. J. Thermoelectric power generation. Thermoelectrics Handbook. CRC Press, Boca Raton, FL; 2005. p. 9-1–9-26.
22. Snyder, G., and Ursell, T. Thermoelectric efficiency and compatibility. *Phys Rev Lett* 2003;91.

Please provide volume number.

Please provide author names and journal title.

Please verify provided page numbers.

Please provide volume number.

23. Snyder, G. J. Thermoelectrics and its energy harvesting: Materials, preparation, and characterization in thermoelectrics 2012.
24. Seifert, W., Pluschke, V., Goupil, C., Zabrocki, K., Müller, E., and Snyder, G. J. Maximum performance in self-compatible thermoelectric elements. *J Mater Res* 2011;26:1933–9.
25. Hung, L. T., Van Nong, N., Han, L., Bjørk, R., Ngan, P. H., Holgate, T. C. et al. Segmented thermoelectric oxide-based module for high-temperature waste heat harvesting. *Energy Technol* 2015;3:1143–51.
26. Souma, T., Ohtaki, M., Shigeno, M., Ohba, Y., Nakamura, N., and Shimozaki, T. Fabrication and power generation characteristics of p-$NaCo2O_4$ n-ZnO oxide thermoelectric modules 2006.
27. Souma, T., Ohtaki, M., Ohnishi, K., Shigeno, M., Ohba, Y., Shimozaki, T. Power generation characteristics of oxide thermoelectric modules incorporating nanostructured ZnO sintered materials. *2007 26th International Conference on Thermoelectrics* 2007:38–41.
28. Thermoelectric power generation using Li-doped NiO and (Ba, Sr)PbO_3 module.
29. Matsubara, I., Funahashi, R., Takeuchi, T., Sodeoka, S., Shimizu, T., and Ueno, K. Fabrication of an all-oxide thermoelectric power generator. *Appl Phys Lett* 2001;78:3627.
30. Funahashi, R., Urata, S., Mizuno, K., Kouuchi, T., and Mikami, M. $Ca_{2.7}Bi_{0.3}Co_4O_9/La_{0.9}Bi_{0.1}NiO_3$ thermoelectric devices with high output power density. *Appl Phys Lett* 2004;85:1036.
31. Reddy, E. S., Noudem, J. G., Hebert, S., and Goupil, C. Fabrication and properties of four-leg oxide thermoelectric modules. *J Phys D Appl Phys* 2005;38:3751–5.
32. Funahashi, R., Mikami, M., Mihara, T., Urata, S., and Ando, N. A portable thermoelectric-power-generating module composed of oxide devices. *J Appl Phys* 2006;99:66117.
33. Urata, S., Funahashi, R., and Mihara, T. Power generation of p-type $Ca_3Co_4O_9$/n-type $CaMnO_3$ module. *2006 25th International Conference on Thermoelectrics* 2006:501–4.
34. Funahashi, R., and Urata, S. Fabrication and application of an oxide thermoelectric system. *Int J Appl Ceram Technol* 2007;4:297–307.
35. Urata, S., Funahashi, R., Mihara, T., Urata, R., Mihara, T. S., and Funahashi, R. Power generation of p-type $Ca_3Co_4O_9$/n-type $CaMnO_3$ module. *2006 25th International Conference on Thermoelectrics* 2006:501–4.
36. Park, K., Choi, J. W., and Lee, C. W. Characteristics of thermoelectric power modules based on p-type $Na(Co_{0.95}Ni_{0.05})_2O_4$ and n-type $Zn_{0.99}Sn_{0.01}O$. *J Alloys Compd* 2009;486:785–9.
37. Tomeš, P., Robert, R., Trottmann, M., Bocher, L., Aguirre, M. H., Bitschi, A. et al. Synthesis and characterization of new ceramic thermoelectrics implemented in a thermoelectric oxide module. *J Electron Mater* 2010;39:1696–703.
38. Choi, S.-M., Lee, K-.H., Lim, C.-H., and Seo, W.-S. Oxide-based thermoelectric power generation module using p-type $Ca_3Co_4O_9$ and n-type $(ZnO)_7In_2O_3$ legs. *Energy Convers Manag* 2011;52:335–9.
39. Lim, C.-H., Choi, S.-M., Seo, W.-S., and Park, H.-H. A power-generation test for oxide-based thermoelectric modules using p-type $Ca_3Co_4O_9$ and n-Type $Ca_{0.9}Nd_{0.1}MnO_3$ legs. *J Electron Mater* 2011;41:1247–55.

Please provide journal title and volume and page numbers.

Please provide journal title and volume and page numbers.

Please provide author names, journal title, volume and page numbers, and reference date.

40. Inagoya, A., Sawaki, D., Horiuchi, Y., Urata, S., Funahashi, R., and Terasaki, I. Thermoelectric module made of perovskite cobalt oxides with large thermopower. *J Appl Phys* 2011;110:123712.
41. Han, L., Jiang, Y., Li, S., Su, H., Lan, X., Qin, K. et al. High temperature thermoelectric properties and energy transfer devices of $Ca_3Co_{4-x}Ag_xO_9$ and $Ca_{1-y}Sm_yMnO_3$. *J Alloys Compd* 2011;509:8970.
42. Funahashi, R. Waste heat recovery using thermoelectric oxide materials. *Sci Adv Mater* 2011;3:682–6.
43. Park, K., and Lee, G. W. Fabrication and thermoelectric power of π-shaped $Ca_3Co_4O_9$/$CaMnO_3$ modules for renewable energy conversion. *Energy* 2013;60:87–93.
44. Mele, P., Kamei, H., Yasumune, H., Matsumoto, K., and Miyazaki, K. Development of thermoelectric module based on dense $Ca_3Co_4O_9$ and $Zn_{0.98}Al_{0.02}O$ legs. *Met Mater Int* 2014;20:389–97.
45. Saucke, G., Populoh, S., Thiel, P., Xie, W., Funahashi, R., and Weidenkaff, A. Compatibility approach for the improvement of oxide thermoelectric converters for industrial heat recovery applications. *J Appl Phys* 2015;118:1–8. doi:10.1063/1.4926476.
46. Van Nong, N., Pryds, N., Linderoth, S., and Ohtaki, M. Enhancement of the thermoelectric performance of p-type layered oxide $Ca_{(3)}Co_{(4)}O_{((9)+delta)}$ through heavy doping and metallic nanoinclusions. *Adv Mater* 2011;23:2484–90.
47. Cobble, M. Calculations of generator performance. *CRC Handbook of Thermoelectrics*, vol. 2, CRC Press, Boca Raton, FL; 1995.
48. Heikes, R. R., and Ure, R. W. Thermoelectricity: Science and engineering. Interscience Publishers, Genva; 1961.
49. Caillat, T., Fleurial, J.-P., Snyder, G. J., and Borshchevsky, A. Development of high efficiency segmented thermoelectric *unicouples. Proceedings of ICT2001: 20the International Conference on Thermoelectrics.* (Cat. No.01TH8589):282–5.
50. Hung, L. T., Van Nong, N., Linderoth, S., and Pryds, N. Segmentation of low-cost high efficiency oxide-based thermoelectric materials. *Phys Status Solidi Appl Mater Sci* 2015;212:767–74.
51. Tecteg Power Generator. http://tecteg.com/.

Please provide reference date and volume numb

Please provide reference date.